

Diffusion-based Time Series Imputation and Forecasting with Structured State Space Models

Juan Miguel Lopez Alcaraz and Nils Strodthoff

Abstract—The imputation of missing values represents a significant obstacle for many real-world data analysis pipelines. Here, we focus on time series data and put forward SSSD, an imputation model that relies on two emerging technologies, (conditional) diffusion models as state-of-the-art generative models and structured state space models as internal model architecture, which are particularly suited to capture long-term dependencies in time series data. We demonstrate that SSSD matches or even exceeds state-of-the-art probabilistic imputation and forecasting performance on a broad range of data sets and different missingness scenarios, including the challenging blackout-missing scenarios, where prior approaches failed to provide meaningful results.

Keywords— Time series, Probabilistic Imputation, Forecasting, Generative Models.

I. INTRODUCTION

Missing input data is a common phenomenon in real-world machine learning applications, which can have many different reasons, ranging from inadequate data entry over equipment failures to file losses. Handling missing input data represents a major challenge for machine learning applications as most algorithms require data without missing values to train. Unfortunately, the imputation quality has a critical impact on downstream tasks, as demonstrated in prior work [43], and poor imputations can even introduce bias into the downstream analysis [51], which can potentially call into question the validity of the results achieved in them.

In this work, we focus on time series data as a data modality, where missing data is particularly prevalent, for example, due to faulty sensor equipment. We will consider a range of different missingness scenarios, see Fig. 4 for a visual overview. The former example suggests that not-at-random missingness scenarios are significant for real-world scenarios. Furthermore, we would like to stress that time series forecasting is a case of blackout missingness, where the location of the imputation window is at the end of the sequence. We also stress that the most realistic scenario to address imputation as an underspecified problem class is the use of probabilistic imputation methods, which do not provide only a single imputation but instead allow samples of different plausible imputations, thus allowing for investigation of the sensitivity of downstream algorithms of the imputed parts, which represents one of the cornerstones of perturbation-based explainable AI methods [10]. Finally, the broadness of prediction intervals provides a way of quantifying the inherent uncertainty in the data.

There is a large body of literature on time series imputation, see [38] for a review, ranging from statistical methods [30] to autoregressive models [2, 4]. Recently, deep generative models started to emerge as a promising paradigm to model time series imputation of long sequences or time series forecasting problems at long horizons. However, many existing models remain limited to the random missing scenario or show unstable behavior during training. Even more striking, we demonstrate

JMLA and NS are with University of Oldenburg, Oldenburg, Germany (email: juan.lopez.alcaraz@uol.de and nils.strodthoff@uol.de). Corresponding author: NS.

that that state-of-the-art approaches even fail to deliver qualitatively meaningful imputations in blackout missing scenarios on certain data sets.

In this work, we aim to address these shortcomings by proposing a new generative-model-based approach for time series imputation. We use diffusion models, and more specifically, the DiffWave framework [26] put forward in the context of speech generation, as the current state-of-the-art in terms of generative modeling in different data modalities. The second principal component of our approach is the use of structured state-space models [19] instead of dilated convolutions or transformer layers as main computational building block of the model, which are particularly suited to handling long-term-dependencies in time series data.

To summarize, our main contributions are as follows: (1) We put forward a combination of state-space models as ideal building blocks to capture long-term dependencies in time series with (conditional) diffusion models as the current state-of-the-art technology for generative modeling. (2) We suggest modifications to the contemporary diffusion model architecture DiffWave[26] to enhance its capability for time series modeling. In addition, we propose a simple yet powerful methodology in which the noise of the diffusion process is introduced just to the regions to be imputed. (3) We provide extensive experimental evidence for the superiority of the proposed approach compared to state-of-the-art approaches on different data sets for various missingness approaches, particularly for the most challenging blackout and forecasting scenarios.

II. STRUCTURED STATE SPACE DIFFUSION (SSSD) MODELS FOR TIME SERIES IMPUTATION

Time series imputation: As per time series data, let x_0 be a data sample with a shape of $\mathbb{R}^{L \times K}$ where L represents the number of time steps, and K represents the number of features or channels. Imputation targets are then typically specified in terms of binary masks that match the shape of the input data, i.e., $m_{\text{imp}} \in [0, 1]^{L \times K}$, where the conditioned values are ones, and zeros denote values to be imputed. In the case where there are also missing values in the input, one additionally requires a mask m_{mvi} of the same shape to distinguish values that are present in the input data (1) from those that are not (0).

In the literature, see, e.g., [30], one distinguishes different missingness scenarios, which we repeat for completeness: We define *random missing (RM)* as a situation where the zero-entries of an imputation mask are sampled randomly according to a uniform distribution across all channels of the whole input sample. Secondly, *missing not at random (MNR)* assumes a missing random subset of x_i in a x_0 at the L dimension at a single K for each K . Finally, *blackout missing (BM)* assumes that there is a missing subset of x_i in a x_0 at the L dimension for all K . As mentioned earlier, *time series forecasting (TF)* is a particular case of BM imputation, where the imputation region spans a consecutive region of t time steps, where t denotes the forecasting horizon across all channels located at the very end of the sequence. For this work, we introduce the consistent coloring scheme used throughout this work; signals is in blue, where the white background represents the conditioned ground truth, whereas the gray

background represents the target signal. Prediction bands derived from imputations represent quantiles from 0.05 to 0.95 as lighter shaded green and from 0.25 to 0.75 as darker shaded green. As these bands do not allow visually assessing the quality of individual imputations, we always additionally show a randomly selected single imputation sample in orange. We refer to our multimedia appendix which contains plots to demonstrate all four missing scenarios.

Diffusion models: Diffusion models [45] represent a class of generative models that demonstrated state-of-the-art performance on a range of different data modalities, ranging from image [11, 21, 22] over speech [7, 26] to video data [23].

Diffusion models learn a mapping from latent space to signal space by sequentially learning to remove noise in a backward process that was added sequentially in a Markovian fashion during a so-called forward process. These two processes, therefore, represent the backbone of the diffusion model. For simplicity, we restrict the unconditional case at the beginning of this section and discuss modifications for the conditional case towards the end. The forward process is parameterized as

$$q(x_1, \dots, x_T | x_0) = \prod_{t=1}^T q(x_t | x_{t-1}), \quad (1)$$

where $q(x_t | x_{t-1}) = \mathcal{N}(x_t; \sqrt{1 - \beta_t} x_{t-1}, \beta_t \mathbb{1})$ and the (fixed or learnable) forward-process variances β_t adjust the noise level. Equivalently, x_t can be expressed in closed form as $x_t = \sqrt{\alpha_t} x_0 + (1 - \alpha_t) \epsilon$ for $\epsilon \sim \mathcal{N}(0, \mathbb{1})$, where $\alpha_t = \sum_{i=1}^t (1 - \beta_i)$.

The backward process is parameterized as

$$p_\theta(x_0, \dots, x_{t-1} | x_T) = p(x_T) \prod_{t=1}^T p_\theta(x_{t-1} | x_t) \quad (2)$$

where $x_T \sim \mathcal{N}(0, \mathbb{1})$. Again, $p_\theta(x_{t-1} | x_t)$ is assumed as normal-distributed (with diagonal covariance matrix) with learnable parameters. Using a particular parameterization of $p_\theta(x_{t-1} | x_t)$, Ho et al. [21] showed that the reverse process can be trained using the following objective,

$$L = \min_\theta \mathbb{E}_{x_0 \sim \mathcal{D}, \epsilon \sim \mathcal{N}(0, \mathbb{1}), t \sim \mathcal{U}(1, T)} \quad (3) \\ ||\epsilon - \epsilon_\theta(\sqrt{\alpha_t} x_0 + (1 - \alpha_t) \epsilon, t)||_2^2,$$

where \mathcal{D} refers to the data distribution and $\epsilon_\theta(x_t, t)$ is parameterized using a neural network. This objective can be seen as a weighted variational bound on the negative log-likelihood that down-weights the importance of terms at small t , i.e., at small noise levels.

Extending the unconditional diffusion process described so far, one can consider conditional variants where the backward process is conditioned on additional information, i.e. $\epsilon_\theta = \epsilon_\theta(x_t, t, c)$, where the precise nature of the conditioning information c depends on the application at hand and ranges from global labels to spectrograms [26]. In our case, it is given by the concatenation of input (masked according to the imputation mask) and the imputation mask itself, i.e., $c = \text{Concat}(x_0 \odot (m_{\text{imp}} \odot m_{\text{mvi}}), (m_{\text{imp}} \odot m_{\text{mvi}}))$, where \odot denotes point-wise multiplication. In this work, we consider two different setups, denoted as D_0 and D_1 , respectively, where we apply the diffusion process to the full signal or to the regions to be imputed only. In any case, the evaluation of the loss function in Eq. (3) is only supposed to be on the input values, where ground truth is available, i.e. where $m_{\text{mvi}} = 1$. For D_0 , this can be seen as a reconstruction loss for the input values corresponding to non-zero portions of the imputation mask (where conditioning is available) and an imputation loss corresponding to input tokens at which the imputation mask vanishes, c.f. also [12]. For D_1 , the reconstruction loss vanishes by construction.

As Tashiro et al. [46], we base our parameterization of $\epsilon_\theta(x_t, t, c)$ on the DiffWave architecture [26]. Different from Tashiro et al. [46],

we do not work with an extended four-dimensional internal representation of shape (batch dimension, diffusion dimension, input channel dimension, time dimension), which necessitates processing time and feature dimensions alternatively since many modern architectures for sequential data, such as transformers or structured state space models, to be discussed below, are only able to process sequential, i.e. three-dimensional input batches. We take the conceptionally simpler path of mapping the input channels into the diffusion dimension and performing only diffusion along the time dimension, i.e. processing batches of shape (batch dimension, diffusion dimension, time dimension). Additionally, we modify the internals of the DiffWave architecture using S4 layers [19] that are better suited to processing time series data than the dilated convolutions used in the original architecture. We postpone a detailed discussion of the model architecture in the proposed approaches section.

State space models: The recently introduced structured state-space model (SSM) [19] represent a very promising modeling paradigm to capture in particular long-term dependencies in time series. At its heart, the formalism draws on a linear state space transition equation, connecting a one-dimensional input sequence $u(t)$ to a one-dimensional output sequence $y(t)$ via a N -dimensional hidden state $x(t)$. Explicitly, this transition equation reads

$$x'(t) = Ax(t) + Bu(t) \text{ and } y(t) = Cx(t) + Du(t), \quad (4)$$

where A, B, C, D are transition matrices. After discretization, the relation between input and output can be written as a convolution operation that can be evaluated efficiently on modern GPUs [19]. The ability to capture long-term dependencies relates to a particular initialization of $A \in \mathbb{R}^{N \times N}$ according to HiPPO theory [18, 20]. In [19], the authors put forward a Structured State Space sequence model (S4) by stacking several copies of the above SSM blocks with appropriate normalization layers and point-wise fully-connected layers in the style of a transformer layer, demonstrating excellent performance on various sequence classification tasks. In fact, the resulting S4 layer parameterizes a shape-preserving mapping of data with shape (batch, model dimension, length dimension) and can therefore be used as a drop-in replacement for transformer, RNN or one-dimensional convolution layers (with appropriate padding). Building on the S4 layer, the authors presented SaShiMi, a generative model architecture for sequence generation [16] obtained by combining S4 layers in a U-net-inspired configuration. While the model was proposed as an autoregressive model, the authors already pointed out the ability to use the (non-causal) SaShiMi as a component in state-of-the-art non-autoregressive models such as DiffWave [26].

Proposed approaches: We propose three different variants of Diffwave-based [26] diffusion models. First, we put forward SSSD^{S4}, a conditional DiffWave-variant [26], which instead of bidirectional dilated convolutions, we have replaced and adapted an S4 layer as a diffusion layer within each of its residual blocks after adding the diffusion embedding. As a second modification, we include a second S4 layer after the addition assignment with the conditional information, which gives the model additional flexibility after joining processed inputs and the conditional information. The effectiveness of this modification is demonstrated in an ablation study in the technical appendix. The architecture is depicted schematically in Figure 1. Second, under the name SSSD^{SA} we explore an extension of the non-autoregressive of the SaShiMi architecture for time series imputation through appropriate conditioning. Third, we investigate CSDI^{S4}, a modification of the CSDI [46] architecture, where we replace the transformer layer operating in the time direction by an S4 model. In this way, we aim to assess potential improvements of an architecture that is more adapted to the domain of time series. A more detailed discussion of the model internals including hyper-parameter settings can be found in the technical appendix.

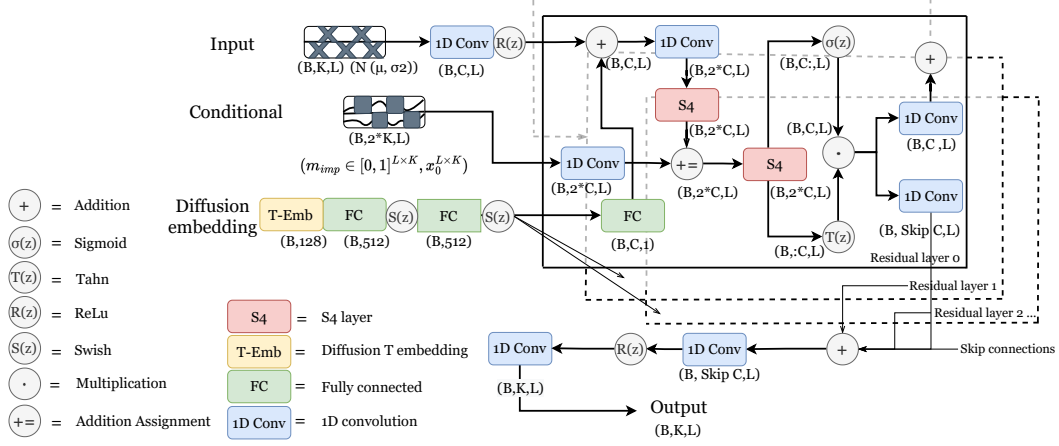


Figure 1. Proposed SSSD^{S4} model architecture.

III. RELATED WORK

Deep-learning based time series imputation: Time series imputation is a very rich topic. A complete discussion— even of the deep learning literature alone— is clearly beyond the scope of this work, and we refer the reader to a recent review on the topic [14]. Deep-learning-based time series imputation methods can be broadly categorized based on the technology used: (1) RNN-based approaches such as BRITS [5], GRU-D [6], NAOMI [31], and M-RNN [50] use single or multi-directional RNNs to model the time series. However, these algorithms suffer of diverse training limitation, and as pointed out in recent works, many of them might only show sub-optimal performance across diverse missing scenarios and at different missing ratios [9] [12]. (2) Generative models represent the second dominant approach in the field. This includes GAN-based approaches such as E^2 -GAN [34], and GRUI-GAN [33] or VAE-based approaches such as GP-VAE [15]. Many of these were found to suffer from unstable training and failed to reach state-of-the-art performance [12]. Recently, also diffusion models such as CSDI [46], the closest competitor to our work, were explored with very strong results. (3) Finally, there is a collection of approaches relying in modern architectures such as graph neural networks (GRIN)[9], and permutation equivariant networks (NRTSI)[44], *self-attention* to capture temporal and feature correlations (SAITS) [12], controlled differential equations networks (NeuralCDE)[36] and ordinal differential equations networks (LatentODE)[40].

Conditional generative modeling with diffusion models:

Diffusion models have been used for related tasks such as inpainting, in particular in the image domain [41, 32]. With appropriate modifications, such methods from the image domain are also directly applicable in the time series domain. Sound is a very special time series, and diffusion models such as DiffWave [26] conditioned on different global labels or Mel spectrograms showed excellent performance in different speech generation tasks. Returning to general time series, as already discussed above, the closest competitor is CSDI [46]. CSDI and this work represent diffusion models and can be seen as DiffWave-variants. The main differences between the two approaches are (1) using SSMs instead of transformers (2) the conceptually more straightforward setup of a diffusion process in time direction only as opposed to feature and time direction, see also the discussion in the proposed approaches section. (3) a different training objective to denoise just the segments to be imputed (D_1). In all of our experiments, we compare to CSDI to demonstrate our approach’s superiority and that exchanging single components (as for CSDI^{S4}) is not sufficient.

Time series forecasting: As mentioned above, time series forecasting can be seen as a special case of time series imputation in a blackout missing scenario. The literature on time series forecasting is even richer than the literature on time series imputation. From one side there are recurrent common place architectures such as LSTNet[27], and LSTMa [3], and from the other side there are modern architectures such as the very recent transformer-based Informer [52] with encoder-decoder design, which showed excellent performance on long-sequence forecasting. Similarly, diverse methods significantly contributed to the literature such as GP-Copula [42], Transformer MAF [39], and TLAE [37].

IV. EXPERIMENTS

A. Experimental protocol

As already discussed above, we do not keep the (input) channel dimension as an explicit dimension during the diffusion process but only keep it implicitly by mapping the channel dimension to the diffusion dimension. This is inspired by the original DiffWave approach, which was designed for single-channel audio data. As we will demonstrate below, this approach leads to outstanding results in scenarios where the number of input channels remains limited to less than about 100 input channels, which covers for example typical single-patient sensor data such as ECG, EEG in the healthcare domain. For more input channels, the model often fails to converge and one has to resort to different training strategies, e.g., by splitting the input channels, and as we will also demonstrate below, this approach without any further modifications already leads to competitive results on data sets with a few hundred input channels, but can certainly be improved by more elaborate procedures and is therefore not within the main scope of this work. For this reason also the mains experimental evaluation of our work focuses on data sets with less than 100 input channels.

Throughout this section, we always train and evaluate imputation models on identical missingness scenarios and ratios, e.g., we train on 20% RM and evaluate based on the same setting. The training on the models was performed on single NVIDIA A30 cards. The motivation for the diversity of data sets in our research is that we look forward to showing the robustness of our proposed methods, specially SSSD^{S4} across diverse qualitative data and diverse baselines, for which we carried out experiments on a health-care-related data set to demonstrate our method trustworthiness in scenarios of high importance. There are diverse performance metrics utilized in this work (where in all cases lower scores signify better imputation results),

most of them involve comparing single imputations to the ground truth, others, incorporate imputations distribution and are therefore specific to probabilistic imputers. We refer to our technical appendix for a discussion on them. Similarly, we present small and concise tables in the main text to support our claims. We refer to the technical appendix for more results, including additional baselines, further details on data sets and preprocessing procedures.

B. Time series imputation

SSSD^{S4} outperforms state-of-the-art imputers on the proposed PTB-XL ECG data set: As first data set, we consider electrocardiogram (ECG) data from the *PTB-XL data set* [47, 48, 17]. ECG data represents an interesting benchmark case as producing coherent imputations beyond the random missing scenario requires to capture the consistent periodic structure of the signal across several beats. We preprocessed the ECG signals at a sampling rate of 100 Hz and considered $L = 250$ time steps (248 in the case of SSSD^{SA}). We considered three different missingness scenarios, RM, NRM, and BM. We present the investigated diffusion model variants, such as CSDI^{S4}, SSSD^{SA}, and SSSD^{S4}, where applicable both for training objectives D_0 and D_1 . As baselines we consider the deterministic LAMC [8], CSDI [46] as a strong probabilistic baseline and a conditional adaptation of the original DiffWave architecture. We report averaged MAE, RMSE, and CRPS for 10 samples generated for each sample in a test sub-set.

Table I
IMPUTATION FOR RM, MNR AND BM SCENARIOS ON THE PTB-XL DATA SET (EXTRACTS, SEE TAB. XIX FOR FURTHER BASELINE AND SETTINGS COMPARISONS).

Model	MAE	RMSE	CRPS
20% RM on PTB-XL			
LAMC	0.0678	0.1309	0.6828
CSDI	0.0038 \pm 2e-6	0.0189 \pm 5e-5	0.0265 \pm 6e-6
CSDI^{S4}	0.0031\pm1e-7	0.0171 \pm 6e-4	0.0202\pm1e-5
SSSD ^{SA}	0.0045 \pm 3e-7	0.0181 \pm 4e-6	0.0314 \pm 7e-5
SSSD^{S4}	0.0034\pm4e-6	0.0119\pm1e-4	0.0282 \pm 1e-3
20% MNR on PTB-XL			
LAMC	0.0759	0.1498	0.8345
CSDI	0.0186 \pm 1e-5	0.0435 \pm 2e-4	0.1306 \pm 5e-5
CSDI^{S4}	0.0222\pm2e-5	0.0573 \pm 1e-3	0.1392 \pm 4e-2
SSSD ^{SA}	0.0170 \pm 1e-4	0.0492 \pm 1e-2	0.1152 \pm 1e-5
SSSD^{S4}	0.0103\pm3e-3	0.0226\pm9e-4	0.0787\pm3e-3
20% BM on PTB-XL			
LAMC	0.0840	0.1171	0.9999
CSDI	0.1054 \pm 4e-5	0.2254 \pm 7e-5	0.7468 \pm 2e-4
CSDI^{S4}	0.0792\pm2e-4	0.1879 \pm 1e-4	0.6222 \pm 6e-4
SSSD ^{SA}	0.0435 \pm 3e-3	0.1167 \pm 1e-2	0.3181 \pm 1e-2
SSSD^{S4}	0.0324\pm3e-3	0.0832\pm8e-3	0.2689\pm3e-3

Across all model types and missingness scenarios, applying the diffusion process to the portions of the sample to be imputed (D_1) consistently yields better results than the diffusion process applied to the entire sample (D_0). In the following, we will therefore restrict ourselves to the D_1 setting. The proposed SSSD^{S4} outperforms the rest of the imputer models by a significant margin in most scenarios, in particular for BM, where we find a reduction in MAE of more than 50% compared to CSDI. On the BM scenario, SSSD^{S4} presents a small difference of cumulative distribution function (CDF) of the imputations against the targets CDF by a CRPS of 0.2689, whereas CSDI obtains 0.746. Similarly, we note that DiffWave as a baseline shows very strong results, which are in some scenarios on par with the technically more advanced SSSD^{SA}, nevertheless, the proposed SSSD^{S4} demonstrate a clear improvement for time series imputation and generation across all the settings. Also, there is a clear improvement that the S4 layer on CSDI^{S4} provides to CSDI across RM and BM settings, especially for the RM scenario where CSDI^{S4} outperforms the rest of methods with lower MAE and CRPS. We hypothesize that the CSDI-approach

is helpful in the RM setting, where consistency across features and time has to be reached, whereas SSSD^{S4} and its variants show clear advantages for MNR and BM (and TF as discussed below) where modeling the time dependence is of primary importance.

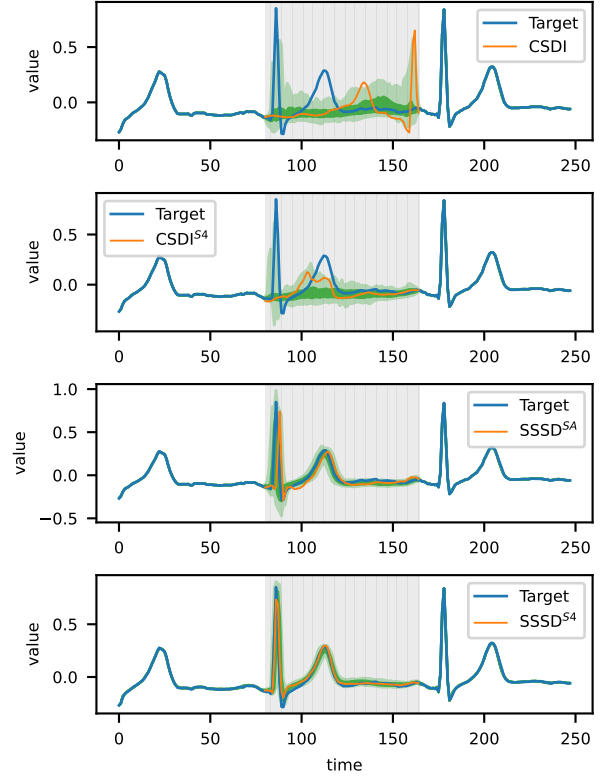


Figure 2. PTB-XL BM imputations for V5 lead of an ECG from a healthy patient.

Existing approaches fail to produce meaningful BM imputations: Fig. 2 shows imputations on a BM scenario for a subset of models from the PTB-XL imputation task. The main purpose is to demonstrate that the achieved improvements through the proposed approaches lead to superior samples in a way that is even apparent to the naked eye. The top left figure demonstrates that the state-of-the-art imputer is unable to produce any meaningful imputations (as visible both from the shaded quantiles as well as from the exemplary imputation). As an example, the identification of a QRS complex with a duration inside the range of 0.08 sec to 0.12 sec is considered as normal signals, however, the model fails to detect the complex and rather shows a misplaced R peak. The imputation quality improves qualitatively with the proposed CSDI^{S4} variant but still misses essential signal features. Only the two proposed SSSD^{SA} and SSSD^{S4} models capture all essential signal features. The qualitatively best result is achieved by SSSD^{S4}, which excels at the task and shows well-controlled quantile bands as expected for a normal ECG sample.

SSSD^{S4} shows competitive imputation performance compared to state-of-the-art approaches on other data sets and high missing ratios: To demonstrate that the excellent performance of SSSD^{S4} extends to further data sets, we collected the MuJoCo data set [40] from [44] to test SSSD^{S4} on highly sparse RM scenarios such as 70%, 80%, and 90%, for which we compare performance against the baselines RNN GRU-D [6], ODE-RNN [40], NeuralCDE [36], Latent-ODE [40], NAOMI [31], and NRTSI [44].

We report an averaged MSE for a single imputation per sample on the test set over 3 trials. All baselines results were collected from [44].

Table II

IMPUTATION MSE RESULTS FOR THE MUJOCo DATA SET. HERE, WE USE A CONCISE ERROR NOTATION WHERE THE VALUES IN BRACKETS AFFECT THE LEAST SIGNIFICANT DIGITS E.G. $0.572(12)$ SIGNIFIES 0.572 ± 0.012

Model	70% RM	80% RM	90% RM
RNN GRU-D	11.34e-3	14.21e-3	19.68e-3
ODE-RNN	9.86e-3	12.09e-3	16.47e-3
NeuralCDE	8.35e-3	10.71e-3	13.52e-3
Latent-ODE	3.00e-3	2.95e-3	3.60e-3
NAOMI	1.46e-3	2.32e-3	4.42e-3
NRTSI	0.63e-3	1.22e-3	4.06e-3
SSSD^{S4}	0.59(8)e-3	1.00(5)e-3	1.90(3)e-3

Table II shows the empirical RM results on the MuJoCo data set, where SSSD^{S4} outperformed all the baselines for all the missingness scenarios, specially, on the highest RM ratio 90% where we achieved with SSSD^{S4} a error reduction of more than 50%, we hypothesize that a small proportion of conditional values is sufficient for SSSD^{S4} be able to properly reconstruct from the backward denoising process time series signals as clearly demonstrated on the experiment.

SSSD^{S4} performance on high-dimensional data sets: We also explore the potential of SSSD^{S4} on data sets with more than 100 channels, following the simple but still sub-optimal channel splitting strategy described above.

We implemented the RM imputation task on the Electricity data set [13] from [12] which contains 370 features at different missingness ratios such as 10%, 30% and 50%. As baselines, M-RNN [50], GP-VAE [15], BRITS [5], SAITS [12] and a transformer variant from [12]. We report an averaged MAE, RMSE, and MRE from one sample generated per test sample over a 3 trial period.

Table III

50% RM IMPUTATION RESULTS FOR THE ELECTRICITY DATA SET (EXTRACTS, SEE TABLE XX FOR FURTHER SETTINGS COMPARISON).

Model	MAE	RMSE	MRE
M-RNN	1.283	1.902	68.7%
GP-VAE	1.097	1.572	58.8%
BRITS	1.037	1.538	55.5%
Transformer	0.895	1.410	47.9%
SAITS	0.876	1.377	46.9%
SSSD^{S4}	0.532(1)	0.821(1)	28.5(1)%

Overall, SSSD^{S4} excelled at the imputation task, demonstrating significant error reductions against the strongest baseline SAITS, as example table Table III contains the results of the on the 50% RM imputation task, where SAITS presented 0.876, 1.377, and 49.9% of MAE, RMSE, and MRE respectively, while we achieved with SSSD^{S4} 0.532, 0.821, and 28.5%, representing outstanding error reductions of 39.3%, 40.4%, and 39.2% respectively. For the rest of the RM settings, SSSD^{S4} still present significantly error reductions, see Table XX in the technical appendix for details. Similarly, we tested on a 25% RM task from [9] on the PEMS-Bay and METR-LA data sets [29] which contains 325 and 207 features respectively. On the PEMS-Bay data set, SSSD^{S4} outperformed well-established baselines such as MICE [49], rGAIN [35], BRITS [5], and MPGGRU [24] in terms of all three metrics MAE, MSE, and MRE, while it was only superseded by the recently proposed GRIN [9]. On the METR-LA data set, SSSD^{S4} is again outperformed by GRIN but on par with the remaining models. We refer to table Table XXI in the technical appendix for a more in-depth results discussion.

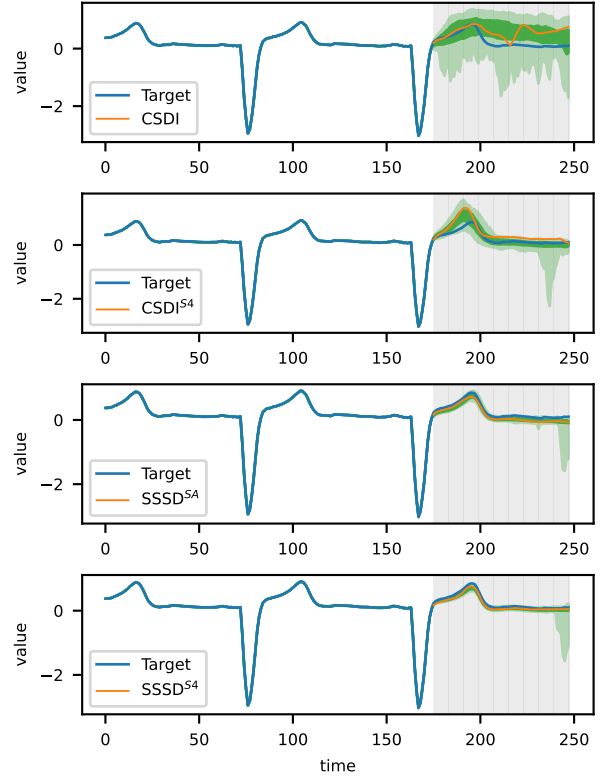


Figure 3. PTB-XL TF for V1 lead of an ECG from a patient with a complete left bundle branch block (CLBBB).

C. Time series forecasting

SSSD^{S4} on proposed data set: We implemented the CSDI, CSDI^{S4}, SSSD^{SA}, and SSSD^{S4} models on two data sets. For both, we report MAE, RMSE, and CRPS as metrics for ten samples generated per test sample in three trials. Firstly, we reconsidered the PTB-XL from before again sampled at 100 Hz, however, for this task at $L = 1000$ time steps per sample, for which we condition on 800 time steps and forecast on 200. SSSD^{SA} outperformed on MAE and CRPS with 0.087 and 0.557 respectively, while SSSD^{S4} achieves slightly larger errors of 0.090 and 0.633. SSSD^{S4} outperformed on RMSE with 0.219, CSDI^{S4} achieved smaller errors than CSDI on the three metrics. Again, the samples presented in Fig. 3 demonstrate a clear improvement that is again even visible with the naked eye.

SSSD^{S4} shows competitive forecasting performance compared to state-of-the-art approaches on various data sets:

We test on the Solar data set collected from GluonTS [1] a forecasting task where the conditional values and forecast horizon are 168 and 24 time steps respectively. As a baselines, we consider CSDI [46], GP-copula [42], Transformer MAF (TransMAF) [39], and TLAE [37]. All baselines results were collected from their original papers. We report an averaged MSE and CRPS of 10 samples generated per test sample over three trials.

Table IV
TIME SERIES FORECASTING RESULTS ON THE SOLAR DATA SET.

Model	MSE	CRPS
GP-copula	$9.8e2 \pm 5.2e1$	0.371 ± 0.022
TransMAF	$9.3e2$	0.368 ± 0.001
TLAE	$6.8e2 \pm 7.5e1$	0.335 ± 0.025
CSDI	$9.0e2 \pm 6.1e1$	0.338 ± 0.012
SSSD^{S4}	$2.7e2 \pm 4.32$	0.219 ± 0.005

The empirical results for the solar data set demonstrate the excellent forecasting capabilities that $SSSD^{S4}$ as we achieved $2.7e-2$ for MSE, where the strongest baseline was TLAE with $6.8e2$, we report a 60% error reduction. Similarly, for the probabilistic metric CRPS, $SSSD^{S4}$ achieved 0.219 while the strongest baseline again TLAE reported 0.335, a significant error reduction of 34% approximately.

Finally, we demonstrate $SSSD^{S4}$'s skillfulness on conventional benchmarking data sets for long-horizon forecasting. We collected the preprocessed ETTm1 data set from [52] and use it for forecasting at five different forecasting settings, where the forecasting length is of 24, 48, 96, 288 and 672 time steps, and the conditional values are 96, 48, 284, 288, and 384 time steps respectively. We compare to LSTnet [27], LSTMa [3], Reformer [25], LogTrans [28], Informer [52] and one of its variants Informer \dagger as baselines. We report an averaged MAE and MSE for a single sample generated for test sample over 2 trials. All baseline results were collected from [52].

Table V
TIME SERIES FORECASTING RESULTS ON THE ETTM1 DATA SET.
(EXTRACTS, SEE TABLE XXIII FOR ERROR ESTIMATES.)

Model	24	48	96	288	672
TF on ETTm1 (MAE)					
LSTNet	1.170	1.215	1.542	2.076	2.941
LSTMa	0.629	0.939	0.913	1.124	1.555
Reformer	0.607	0.777	0.945	1.094	1.232
LogTrans	0.412	0.583	0.792	1.320	1.461
Informer\dagger	0.371	0.470	0.612	0.879	1.103
Informer	0.369	0.503	0.614	0.786	0.926
SSSDS4	0.361	0.479	0.547	0.648	0.783
TF on ETTm1 (MSE)					
LSTNet	1.968	1.999	2.762	1.257	1.917
LSTMa	0.621	1.392	1.339	1.740	2.736
Reformer	0.724	1.098	1.433	1.820	2.187
LogTrans	0.419	0.507	0.768	1.462	1.669
Informer\dagger	0.306	0.465	0.681	1.162	1.231
Informer	0.323	0.494	0.678	1.056	1.192
SSSDS4	0.351	0.612	0.538	0.797	0.804

The experimental results confirm again $SSSD^{S4}$'s robust forecasting capabilities, specifically for long-horizon forecasting, where also the conditional time steps increases. For the first setting, $SSSD^{S4}$ outperformed the rest of the baselines on MAE, while on MSE is only behind Informer \dagger score. For the second setting, on shorter forecast conditional and target lengths $SSSD^{S4}$ scores are comparable with Informer and Informer \dagger , while on the remaining three settings, $SSSD^{S4}$ outperformed the rest of the baselines with significant error reduction, for example for , achieving 0.783 and 0.804 for MAE and MSE, respectively, against the strongest baseline Informer with 0.926 and 1.192, respectively. We recall that this is a challenging setting in which we condition on 384 time steps to forecast 672.

V. CONCLUSION

In this work we proposed the combination of structured state space models as emerging model paradigm for sequential data with long-term dependencies and diffusion models as one of the current state-of-the-art approaches for generative models. The proposed $SSSD^{S4}$ outperforms existing state-of-the-art imputers on various data sets under different missingness scenarios, with particularly strong performance in blackout missing and forecasting scenarios, provided the number of input channels does not grow too large. In particular, we present examples where the qualitative improvement in imputation quality is even apparent to the naked eye. We see the proposed technology as a very promising technology for generative models in the time series domain, which open the possibility to build generative models conditioned on various kinds of information from global labels to local information such as semantic segmentation mask, which in turn enables a broad range of further downstream applications.

ACKNOWLEDGMENT

The authors would like thank the authors of [19, 16] for releasing and maintaining the source code for structured state space models <https://github.com/HazyResearch/state-spaces>. Our Diffwave code builds on the implementation provided by <https://github.com/philsyn/DiffWave-Vocoder>.

REFERENCES

- [1] A. Alexandrov, K. Benidis, M. Bohlke-Schneider, V. Flunkert, J. Gasthaus, T. Januschowski, D. C. Maddix, S. Rangapuram, D. Salinas, J. Schulz, L. Stella, A. C. Türkmen, and Y. Wang. Gluonts: Probabilistic and neural time series modeling in python. *Journal of Machine Learning Research*, 21(116):1–6, 2020. URL <http://jmlr.org/papers/v21/19-820.html>.
- [2] A. Atyabi, F. Shic, and A. J. Naples. Mixture of autoregressive modeling orders and its implication on single trial eeg classification. *Expert systems with applications*, 65:164–180, 2016. doi: 10.1016/j.eswa.2016.08.044.
- [3] D. Bahdanau, K. Cho, and Y. Bengio. Neural machine translation by jointly learning to align and translate. In Y. Bengio and Y. LeCun, editors, *3rd International Conference on Learning Representations, ICLR 2015*, 2015.
- [4] F. Bashir and H.-L. Wei. Handling missing data in multivariate time series using a vector autoregressive model-imputation (var-im) algorithm. *Neurocomput.*, 276(C):23–30, feb 2018. ISSN 0925-2312. doi: 10.1016/j.neucom.2017.03.097. URL <https://doi.org/10.1016/j.neucom.2017.03.097>.
- [5] W. Cao, D. Wang, J. Li, H. Zhou, L. Li, and Y. Li. Brits: Bidirectional recurrent imputation for time series. In *Advances in Neural Information Processing Systems*, volume 31, 2018. URL <https://proceedings.neurips.cc/paper/2018/file/734e6bfcfd358e25ac1db0a4241b95651-Paper.pdf>.
- [6] Z. Che, S. Purushotham, K. Cho, D. Sontag, and Y. Liu. Recurrent neural networks for multivariate time series with missing values, 2016. URL <https://arxiv.org/abs/1606.01865>.
- [7] N. Chen, Y. Zhang, H. Zen, R. J. Weiss, M. Norouzi, and W. Chan. Wavegrad: Estimating gradients for waveform generation. In *International Conference on Learning Representations*, 2020.
- [8] X. Chen, M. Lei, N. Saunier, and L. Sun. Low-rank autoregressive tensor completion for spatiotemporal traffic data imputation. *IEEE Transactions on Intelligent Transportation Systems*, pages 1–10, 2021. doi: 10.1109/TITS.2021.3113608.
- [9] A. Cini, I. Marasca, and C. Alippi. Filling the `g_ap_s`: Multivariate time series imputation by graph neural networks. In *International Conference on Learning Representations*, 2022. URL <https://openreview.net/forum?id=kOu3-S3wJ7>.
- [10] I. Covert, S. Lundberg, and S.-I. Lee. Explaining by removing: A unified framework for model explanation. *Journal of Machine Learning Research*, 22(209):1–90, 2021.
- [11] P. Dhariwal and A. Nichol. Diffusion models beat gans on image synthesis. In *Advances in Neural Information Processing Systems*, volume 34, pages 8780–8794, 2021. URL <https://proceedings.neurips.cc/paper/2021/file/49ad23d1ec9fa4bd8d77d02681df5cfa-Paper.pdf>.
- [12] W. Du, D. Cote, and Y. Liu. SAITS: Self-Attention-based Imputation for Time Series. *arXiv preprint 2202.08516*, 2022.
- [13] D. Dua and C. Graff. UCI machine learning repository, 2017. URL <http://archive.ics.uci.edu/ml>.
- [14] C. Fang and C. Wang. Time series data imputation: A survey on deep learning approaches. *arXiv preprint arXiv:2011.11347*, 2020.
- [15] V. Fortuin, D. Baranchuk, G. Raetsch, and S. Mandt. Gp-vae: Deep probabilistic time series imputation. In *Proceedings of the Twenty Third International Conference on Artificial Intelligence and Statistics*, volume 108 of *Proceedings of Machine Learning Research*, pages 1651–1661, 26–28 Aug 2020. URL <https://proceedings.mlr.press/v108/fortuin20a.html>.

[16] K. Goel, A. Gu, C. Donahue, and C. Re. It's raw! Audio generation with state-space models. In *Proceedings of the 39th International Conference on Machine Learning*, volume 162, pages 7616–7633, 17–23 Jul 2022. URL <https://proceedings.mlr.press/v162/goel22a.html>.

[17] A. L. Goldberger, L. A. N. Amaral, L. Glass, J. M. Hausdorff, P. C. Ivanov, R. G. Mark, J. E. Mietus, G. B. Moody, C.-K. Peng, and H. E. Stanley. PhysioBank, PhysioToolkit, and PhysioNet. *Circulation*, 101(23):e215–e220, 2000. doi: 10.1161/01.CIR.101.23.e215.

[18] A. Gu, T. Dao, S. Ermon, A. Rudra, and C. Ré. Hippo: Recurrent memory with optimal polynomial projections. In *Advances in Neural Information Processing Systems*, volume 33, pages 1474–1487, 2020. URL <https://proceedings.neurips.cc/paper/2020/file/102f0bb6efb3a6128a3c750dd16729be-Paper.pdf>.

[19] A. Gu, K. Goel, and C. Ré. Efficiently modeling long sequences with structured state spaces. In *International Conference on Learning Representations*, 2022.

[20] A. Gu, I. Johnson, A. Timalsina, A. Rudra, and C. Ré. How to train your hippo: State space models with generalized orthogonal basis projections. *arXiv preprint 2206.12037*, 2022. doi: 10.48550/ARXIV.2206.12037. URL <https://arxiv.org/abs/2206.12037>.

[21] J. Ho, A. Jain, and P. Abbeel. Denoising diffusion probabilistic models. In *Advances in Neural Information Processing Systems*, volume 33, pages 6840–6851, 2020. URL <https://proceedings.neurips.cc/paper/2020/file/4c5bcfec8584af0d967f1ab10179ca4b-Paper.pdf>.

[22] J. Ho, C. Saharia, W. Chan, D. Fleet, M. Norouzi, and T. Salimans. Cascaded diffusion models for high fidelity image generation. *J. Mach. Learn. Res.*, 23:47:1–47:33, 2022.

[23] J. Ho, T. Salimans, A. Gritsenko, W. Chan, M. Norouzi, and D. J. Fleet. Video diffusion models. *arXiv preprint 2204.03458*, 2022.

[24] Y. Huang, Y. Weng, S. Yu, and X. Chen. Diffusion convolutional recurrent neural network with rank influence learning for traffic forecasting. In *18th IEEE International Conference On Trust, Security And Privacy In Computing And Communications*, pages 678–685, 2019. doi: 10.1109/TrustCom/BigDataSE.2019.00096. URL <https://doi.org/10.1109/TrustCom/BigDataSE.2019.00096>.

[25] N. Kitaev, L. Kaiser, and A. Levskaya. Reformer: The efficient transformer. In *8th International Conference on Learning Representations, ICLR 2020*, 2020.

[26] Z. Kong, W. Ping, J. Huang, K. Zhao, and B. Catanzaro. Diffwave: A versatile diffusion model for audio synthesis. In *9th International Conference on Learning Representations, ICLR 2021*, 2021. URL <https://openreview.net/forum?id=a-xFK8Ymz5J>.

[27] G. Lai, W.-C. Chang, Y. Yang, and H. Liu. Modeling long- and short-term temporal patterns with deep neural networks. In *The 41st International ACM SIGIR Conference on Research & Development in Information Retrieval*, page 95–104, 2018. doi: 10.1145/3209978.3210006. URL <https://doi.org/10.1145/3209978.3210006>.

[28] S. Li, X. Jin, Y. Xuan, X. Zhou, W. Chen, Y.-X. Wang, and X. Yan. Enhancing the locality and breaking the memory bottleneck of transformer on time series forecasting. In *Advances in Neural Information Processing Systems*, volume 32, 2019. URL <https://proceedings.neurips.cc/paper/2019/file/6775a0635c302542da2c32aa19d86be0-Paper.pdf>.

[29] Y. Li, R. Yu, C. Shahabi, and Y. Liu. Diffusion convolutional recurrent neural network: Data-driven traffic forecasting. In *International Conference on Learning Representations (ICLR '18)*, 2018.

[30] W. Lin and C. Tsai. Missing value imputation: a review and analysis of the literature. *Artificial Intelligence Review*, 53(2):1487–1509, 2020. doi: 10.1007/s10462-019-09709-4. URL <https://link.springer.com/article/10.1007/s10462-019-09709-4>.

[31] Y. Liu, R. Yu, S. Zheng, E. Zhan, and Y. Yue. Naomi: Non-autoregressive multiresolution sequence imputation. In *Advances in Neural Information Processing Systems*, volume 32, 2019. URL <https://proceedings.neurips.cc/paper/2019/file/50c1f44e426560f3f2cdcb3e19e39903-Paper.pdf>.

[32] A. Lugmayr, M. Danelljan, A. Romero, F. Yu, R. Timofte, and L. Van Gool. RePaint: Inpainting using denoising diffusion probabilistic models. In *Computer Vision and Pattern Recognition*, 2022.

[33] Y. Luo, X. Cai, Y. ZHANG, J. Xu, and Y. xiaojie. Multivariate time series imputation with generative adversarial networks. In *Advances in Neural Information Processing Systems*, volume 31, 2018. URL <https://proceedings.neurips.cc/paper/2018/file/96b9bff013acedfb1d140579e2fbeb63-Paper.pdf>.

[34] Y. Luo, Y. Zhang, X. Cai, and X. Yuan. E²gan: End-to-end generative adversarial network for multivariate time series imputation. In *Proceedings of the Twenty-Eighth International Joint Conference on Artificial Intelligence, IJCAI-19*, pages 3094–3100, 7 2019. doi: 10.24963/ijcai.2019/429. URL <https://doi.org/10.24963/ijcai.2019/429>.

[35] X. Miao, Y. Wu, J. Wang, Y. Gao, X. Mao, and J. Yin. Generative semi-supervised learning for multivariate time series imputation. *Proceedings of the AAAI Conference on Artificial Intelligence*, 35(10):8983–8991, May 2021. URL <https://ojs.aaai.org/index.php/AAAI/article/view/17086>.

[36] J. Morrill, C. Salvi, P. Kidger, and J. Foster. Neural rough differential equations for long time series. In *Proceedings of the 38th International Conference on Machine Learning*, volume 139, pages 7829–7838, 18–24 Jul 2021. URL <https://proceedings.mlr.press/v139/morrill21b.html>.

[37] N. Nguyen and B. Quanz. Temporal latent auto-encoder: A method for probabilistic multivariate time series forecasting. *Proceedings of the AAAI Conference on Artificial Intelligence*, 35(10):9117–9125, May 2021. URL <https://ojs.aaai.org/index.php/AAAI/article/view/17101>.

[38] M. S. Osman, A. M. Abu-Mahfouz, and P. R. Page. A survey on data imputation techniques: Water distribution system as a use case. *IEEE Access*, 6:63279–63291, 2018. doi: 10.1109/ACCESS.2018.2877269.

[39] K. Rasul, A. Sheikh, I. Schuster, U. M. Bergmann, and R. Vollgraf. Multivariate probabilistic time series forecasting via conditioned normalizing flows. In *9th International Conference on Learning Representations, ICLR 2021*, 2021.

[40] Y. Rubanova, R. T. Q. Chen, and D. K. Duvenaud. Latent ordinary differential equations for irregularly-sampled time series. In H. Wallach, H. Larochelle, A. Beygelzimer, F. d'Alché-Buc, E. Fox, and R. Garnett, editors, *Advances in Neural Information Processing Systems*, volume 32. Curran Associates, Inc., 2019. URL <https://proceedings.neurips.cc/paper/2019/file/42a6845a557bef704ad8ac9cb4461d43-Paper.pdf>.

[41] C. Saharia, W. Chan, H. Chang, C. A. Lee, J. Ho, T. Salimans, D. J. Fleet, and M. Norouzi. Palette: Image-to-image diffusion models. In *NeurIPS 2021 Workshop on Deep Generative Models and Downstream Applications*, 2021. URL <https://openreview.net/forum?id=c7NBMfDXbW>.

[42] D. Salinas, M. Bohlke-Schneider, L. Callot, R. Medico, and J. Gasthaus. High-dimensional multivariate forecasting with low-rank gaussian copula processes. In *Advances in Neural Information Processing Systems*, volume 32, 2019. URL <https://proceedings.neurips.cc/paper/2019/file/0b105cf1504c4e241fcc6d519ea962fb-Paper.pdf>.

[43] T. Shadbahr, M. Roberts, J. Stanczuk, J. D. Gilbey, P. Teare, S. Dittmer, M. Thorpe, R. V. Torné, E. Sala, P. Lio', M. N. Patel, A.-C. Collaboration, J. H. F. Rudd, T. Mirtti, A. S. Rannikko, J. A. D. Aston, J. Tang, and C.-B. Schonlieb. Classification of datasets with imputed missing values: does imputation quality matter? *arXiv preprint 2206.08478*, 2022.

[44] S. Shan, Y. Li, and J. B. Oliva. Nrtsi: Non-recurrent time series imputation, 2021. URL <https://arxiv.org/abs/2102.03340>.

[45] J. Sohl-Dickstein, E. Weiss, N. Maheswaranathan, and S. Ganguli. Deep unsupervised learning using nonequilibrium thermody-

namics. In *Proceedings of the 32nd International Conference on Machine Learning*, volume 37 of *Proceedings of Machine Learning Research*, pages 2256–2265, 07–09 Jul 2015. URL <https://proceedings.mlr.press/v37/sohl-dickstein15.html>.

[46] Y. Tashiro, J. Song, Y. Song, and S. Ermon. CSDI: Conditional score-based diffusion models for probabilistic time series imputation. *Advances in Neural Information Processing Systems*, 34: 24804–24816, 2021.

[47] P. Wagner, N. Strothoff, R.-D. Bousseljot, D. Kreiseler, F. I. Lunze, W. Samek, and T. Schaeffter. PTB-XL, a large publicly available electrocardiography dataset. *Scientific Data*, 7(1):154, 2020. doi: 10.1038/s41597-020-0495-6. URL <https://doi.org/10.1038/s41597-020-0495-6>.

[48] P. Wagner, N. Strothoff, R.-D. Bousseljot, W. Samek, and T. Schaeffter. PTB-XL, a large publicly available electrocardiography dataset, 2020.

[49] I. R. White, P. Royston, and A. M. Wood. Multiple imputation using chained equations: Issues and guidance for practice. *Stat. Med.*, 30(4):377–399, Feb. 2011.

[50] J. Yoon, W. R. Zame, and M. van der Schaar. Estimating missing data in temporal data streams using multi-directional recurrent neural networks. *IEEE Transactions on Biomedical Engineering*, 66(5):1477–1490, 2019. doi: 10.1109/TBME.2018.2874712.

[51] Z. Zhang, X. Xiao, W. Zhou, D. Zhu, and C. I. Amos. False positive findings during genome-wide association studies with imputation: influence of allele frequency and imputation accuracy. *Human Molecular Genetics*, 31(1):146–155, 2022. doi: 10.1093/hmg/ddab203. URL <https://doi.org/10.1093/hmg/ddab203>.

[52] H. Zhou, S. Zhang, J. Peng, S. Zhang, J. Li, H. Xiong, and W. Zhang. Informer: Beyond efficient transformer for long sequence time-series forecasting. In *The Thirty-Fifth AAAI Conference on Artificial Intelligence, AAAI 2021*, volume 35, pages 11106–11115, 2021.

APPENDIX

A. Training hyperparameters and architectures

Table VI
LAMC HYPER-PARAMETERS

Hyper-parameter	Value
Rhos	0.001, 0.01, 0.1, 1, 2, 3, 5, 10, 20.
Lambdas	0.001, 0.01, 0.1, 1, 2, 3, 5, 6, 8, 10.
Epsilons	1e-4, 1e-3, 1e-2, 1, 2, 5, 8, 10.
Ranks	2, 5, 10, 20, 50, 80, 100.
Iterations	100

LAMC: For the LAMC algorithm, we defined a range of hyper-parameters to be chosen by an exhaustive grid search given the best test metrics. Table VI contains the LAMC hyper-parameter implemented through all the experiments. We decided to implement this algorithm as a baseline due it is a qualitatively different methodologies for time series imputation as our probabilistic diffusion models as it is a matrix auto completion approach. The description of the algorithm methodology goes beyond the scope of our research; however, we invite the reader to search further if desired at [8].

CSDI and CSDI^{S4}: Throughout all our research, the implementation of CSDI [46] as a baseline with the author’s default hyper-parameters settings for training. Similarly, we CSDI^{S4} remained unchanged except for the transformer replacement for an state space model. Table VII contains all the hyper-parameters that conform CSDI and CSDI^{S4} training and architecture. For CSDI^{S4} setting, the S4 model implemented on all of the experiments is a bidirectional single channel setting with layer normalization, no drop-out, and 64 dimensions of the state N , also, a maximum sequence length as required per each D .

Table VII
CSDI HYPER-PARAMETERS

Hyper-parameter	Value
Residual layers	4
Residual channels	64
Diffusion embedding dim.	128
Schedule	Quadratic
Diffusion steps T	50
B_0	0.0001
B_1	0.5
Feature embedding dim.	128
Time embedding dim.	16
Self-attention layers time dim.	1
Self-attention heads time dim.	8
Self-attention layers feature dim.	1
Self-attention heads feature dim.	8
Optimizer	Adam
Learning rate	1×10^{-3}
Weight decay	1×10^{-6}

Table VIII
SSSD^{SA} HYPER-PARAMETERS

Hyper-parameter	Value
Residual layers	6
Pooling factor	[2,2]
Feature expansion	2
Diffusion embedding dim. 1	128
Diffusion embedding dim. 2	512
Diffusion embedding dim. 3	512
Schedule	Linear
Diffusion steps T	200
B_0	0.0001
B_1	0.02
Optimizer	Adam
Learning rate	2×10^{-4}

SSSD^{SA}: Table VIII contains the SSSD^{SA} hyper-parameters for all our experiments. SSSD^{SA} build as a variant of the SaShiMi [16] is a 128-dimensional U-Net model with six residual layers, consisting of an S4 and feed-forward layers in a block manner at each pooling level, where the pooling factor in decreasing the sequence length is 2 and 2 and its respective feature expansion of 2. There is a single three-level diffusion embedding with dimensions 128, 512, and 512, respectively for all of the residual layers. As for S4, a bidirectional single channel setting with layer normalization, no drop-out and 64 dimensions of the state N , also, a maximum sequence length as required per each D , but with a gated linear unit in each layer.

Table IX
SSSD^{S4} HYPER-PARAMETERS

Hyper-parameter	Value
Residual layers	36
Residual channels	256
Skip channels	256
Diffusion embedding dim. 1	128
Diffusion embedding dim. 2	512
Diffusion embedding dim. 3	512
Schedule	Linear
Diffusion steps T	200
B_0	0.0001
B_1	0.02
Optimizer	Adam
Learning rate	2×10^{-4}

SSSD^{S4}: We present in table IX the proposed SSSD^{S4} hyper-parameters and training settings used through all our experiments. SSSD^{S4} a model build from DiffWave [26] it consists of a network

of 36 stacked residual layers with 256 residual and skip channels. Similarly than SSSD^{SA} , SSSD^{S4} have a three level diffusion embedding of 128, 256, and 256 dimensions with a swish activation function over the second and third level. After the addition of diffusion embedding, we implemented a convolutional layer for double the the residual channels dimension of the input, for then compute the first S4 diffusion. Similarly, after a similar expansion of the conditional information and its addition to the input, there is the application of a second S4 layer. Then the output is passed through a gated-tanh for non-linearity, for which we then project back from residual channels to the channel dimensionality with a convolutional layer. We used 200-time steps on a linear schedule for diffusion configuration from a beta of 0.0001 to 0.02. We utilized Adam as an optimizer with a learning rate of 2×10^{-4} . For the S4 model, similarly than the last approaches, bidirectional single channel setting with layer normalization, no drop-out and 64 dimensions of the state N , also, a maximum sequence length as required per each D .

Table X
S4 HYPER-PARAMETERS

Hyper-parameter	Value
Layers	1
State N dimensions	64
Bidirectional	Yes
Layer normalization	Yes
Drop-out	0.0
Maximum length	as required

S4: Finally in this section, we present the hyper-parameter setting for the state space S4 model [19] implemented through all our research. Table X contains the hyper-parameter settings for the S4 state space model implementation, overall, we utilize a single S4 layer with a bidirectional setting for time dependencies learning of series on both directions. Similarly, we applied a layer normalization and utilize a consistent dimensionality of the state N of 64 based on previous studies [19] which demonstrated outstanding results in all our experiments.

Hyper-parameter selection: In this paragraph, we briefly describe the strategy that lead to the hyper-parameter selections discussed in the previous paragraphs: As first remark, we focus on SSSD^{S4} in this section. These settings were applied to SSSD^{SA} without further experimentation and only adapted the number of residual layers to lead to a model with comparable computational complexity as SSSD^{S4} . For CSDI $^{\text{S4}}$, we left the hyper-parameters as close to the original default hyper-parameters as possible. As a general remark, we point out that the hyper-parameter optimization was carried based on validation set scores on the PTB-XL data set at 248 time steps. We did not adjust the hyper-parameters for other data sets, which can be seen as a hint for the robustness of the proposed method. Below, we briefly comment on specific aspects of the hyperparameter selection:
Diffusion hyper-parameters: We implemented a linear schedule with a minimum noise level B_0 of 0.001 and the maximum B_1 as 0.5, based on trial and error. We found that the less diffusion steps, the faster the network converges during training, however, at the cost of less accurate results. In this respect, using 200 diffusion steps represented a reasonable compromise.
Three-level diffusion embedding: From the beginning of our experiments we implemented a three level multidimensional embedding with 128, 512, and 512 units respectively. While reducing the residual layers in some experiments, we also experimented with reducing also those dimensionalities to 16, 32, 32 or 64, 64, 256, however, found that the former choice lead to better results.
Residual channels and skip channels: we introduced large amount of channels (256) to avoid the degradation problem.
Residual layers: We set the number of residual layers to 36 after the experimental phase of our ablation study. In our previous experiments with a single S4 layer, we worked with 48 layers but reduced it to 36 to increase the

speed of convergence during training and to reduce the computational complexity of the overall model, which in variant C requires two S4 layers.

B. Data sets description

Table XI
PTB-XL DATA SET DETAILS

Description / Setting	PTB-XL 248	PTB-XL 1000
Train size	69,764	17,441
Validation size	8,772	2,193
Test size	8,812	2,203
Training batch	32	4
Sample length	248	1000
Sample features	12	12
Conditional values	198	800
Target values	52	200

PTB-XL data set: Table XI contains the PTB-XL data set details [47, 48]. The PTB-XL ECG data set consists of 21837 clinical 12-lead ECGs, each lasting 10 seconds, from 18885 patients. The data set was collected and preprocessed as in the Physionet repository [17], data is already normalized and we presented resulting metrics in this setup. We collected for all experiments the ECG signals at a sampling rate of 100 Hz. For the three imputation and forecasting scenarios we utilize 20% as target values. In all of the settings, the number of input channels is 12 as it is a 12 leads electrocardiogram. The PTB-XL data set contains 21,837 samples for a full sample of 1,000 time steps (10 seconds ECG signal), where 17,441 samples are for training and 2,203 for testing. Validations sets are 8,772, and 2,193 respectively. However, for the 248 time steps setting, the data set was preprocessed on crops, which corresponds to 69,764 training and 8,812 test samples.

Table XII
ELECTRICITY DATA SET DETAILS

Description	Value
Train size	817
Test size	921
Training batch	43
Sample length	100
Data set features	370
Sample features	37
Conditional values	90, 70, 50
Target values	10, 30, 50

Electricity data set: Table XII contains details of the electricity data set for RM imputation. The electricity data set from the UCI repository [13] contains electricity usage data (in kWh) gathered from 370 clients which represent 370 features every 15 minutes. The data set was collected and preprocessed as in SAITS implementation [12] for a fair performance comparison, however, as the data set do not contain missing values, we collected the complete data set and in our experiments we randomly dropped the values for targets computation according to the RM scenario. The data is already normalized and we present results in this setting. The first 10 months of data (2011/01 - 2011/10) are the test set, the following 10 months of data (2011/11 - 2012/08) the validation set and the left (2012/09 - 2014/12) the training set. We directly utilize the training and test set leaving the validation set out. We consider this a challenging task due to most of the features or clients in the test set did not registered electricity consumption, thus, creating samples with consistent values rather than patterns in the signal, which are not present in the training set as the clients reported electricity usage in future dates. The data set contains

817 samples of a length of 100 time steps with the 370 mentioned features. However, we found faster network converging when feature sampling, specifically, splitting the 370 channels into 10 batches of 37 features each, then, passing to the network mini-batches of 43 samples each with 37 features and its respective length of 100 to don't drop any data during training.

Table XIII
MUJOCO DATA SET DETAILS

Description	Value
Train size	8000
Test size	2000
Training batch	50
Sample length	100
Data set features	14
Conditional values	50, 30, 20, 10
Target values	50, 70, 80, 90

MuJoCo data set: Table XIII contains details of the MuJoCo data set, which is a data set for physical simulation, created by the authors at [40] using the "Hopper" model from the Deepmind Control Suite. The hopper's initial placements and speeds are randomly sampled in such a way that the hopper rotates in the air before crashing to the earth. There are 10,000 sequences of 100 regularly sampled time points for each trajectory in the 14-dimensional data set. By convention, there is a 80/20 random split for training and testing. Both sets collected already preprocessed the NRTSI authors repository [44] for a fair metrics comparison.

Table XIV
PEMS-BAY DATA SET DETAILS

Description	Value
Train size	1200
Test size	50
Training batch	40
Sample length	200
Data set features	325
Sample features	65
Conditional values	150
Target values	50

PEMS-BAY data set: Table XIV contains details of the PEMS-Bay data set [24], which was compiled for The Performance Measurement System (PeMS) of the California Transportation Agencies (CalTrans). It is represented by a network of 325 traffic sensors in the California Bay Area, it contains traffic readings every five minutes for six months, from January 1st 2017 to May 31st 2017. The data set was collected and from [9]. The preprocessing from the methodology as the usage of graph neural networks required the creation of an adjacency matrix from the original data set. We work directly with the data set which has 52,116 time steps and 325 features. However, in order to obtain samples for training, we considered 200 time steps over the first 50,000 to get 250 samples, we set the first 240 for training and the 10 rest for testing. Then, we fit a standard scaler with the train set and transform both train and test sets. Finally, we feature sampled to obtain batches by a factor of 5, where for training set we obtained 5 batches of 240 samples with 200 time steps and 65 channels each. Finally, we iterate over the second dimension to pass batches of 40 for training.

METR-LA data set: Table XV contains details of the METR-LA data set, which represents the traffic data from a road network consisting of 207 loop detectors in a period between 1st of March 2012 to the 30th of June 2012. Similar to the preprocessing of the PEMS-Bay data set, we select from the original set the first 34,000

Table XV
METR-LA DATA SET DETAILS

Description	Value
Train size	750
Test size	100
Training batch	50
Sample length	200
Data set features	207
Sample features	40
Conditional values	150
Target values	50

time steps and the first 200 features, we obtained 170 samples of 200 time steps each, we set the 150 first to be training set and the remaining 20 for testing. Finally, we feature sampled by a factor of 5, obtaining for training 5 batches of 150 samples with 200 time steps and 40 features each. For training we iterate over the first dimension to obtain batches of 50 samples.

Table XVI
SOLAR DATA SET DETAILS

Description	Value
Train size	130
Test size	16
Training batch	65
Sample length	192
Data set features	128
Sample features	64
Conditional values	168
Target values	24

Solar data set: Table XVI presents details of the solar data set. The original data set contains the solar power production records in the year of 2006, which is sampled every 10 minutes from 137 photovoltaic power plants in Alabama State [27]. However, for convention, we collected the data set from GluonTS [1] which is hourly sampled. The task is to condition on 168 time steps to forecast the following 24. The whole data set contains 73 samples of 192 time steps and 128 features each in a chronological manner, we set the first 65 as the training set and the remaining 8 as the test set. Similar to the preprocessing applied to other data sets described above, we feature sample this data set by a factor of 2, where for training set, for example, we obtained 2 batches of 65 samples with 192 time steps and 64 features each. We standard scale the train and test sets for training.

Table XVII
ETTM1 DATA SET DETAILS

Description	Value
Train size	33,865, 34,417, 34,000
Test size	11,490, 10,000, 11,420
Training batch	65, 127, 17
Sample length	120, 96, 480
Data set features	7
Conditional values	96, 48, 384
Target values	24, 48, 96

Description	Value
Train size	33,600, 33,200
Test size	10,000, 10,000
Training batch	14, 4
Sample length	576, 1,052
Data set features	7
Conditional values	288, 384
Target values	288, 672

ETTm1 data set: Table XVII contains the ETTm1 data set details. This data set was created to investigate the amount of detail required for long time series forecasting based on the Electricity Transformer Temperature (ETT), which is an important measure for the long-term deployment of electric power. The data set contains information of a compilation of 2-year data from two distinct Chinese counties. Here, we work with ETTm1 which covers data at a 15-minute level. The data is composed of the target value oil temperature and six power load features. We collected and preprocessed the data directly from [52], we forecast in each of the benchmarking horizons, utilizing train and test sets, coming from the original split of train/val/test set, which was for 12/4/4 months, respectively. As seen in table XVII, there are five different preprocessing settings implemented with regard to the forecast horizon, the first table contains information of three and the second for the remaining two, where the main difference is the number of values to condition in a sample and the targets to forecast. Similarly, there are some differences with respect to the batch size used during training. As the sample get longer, we utilize smaller batch sizes, finally, for samples generation, as the test sets are significantly large with more than 10,000 samples each, we subset the test set in order to obtain batches.

C. Additional content

1) S4 Model:

$$A_{nk} = - \begin{cases} (2n+1)^1/2(2k+1)1/2 & \text{if } n > k \\ n+1 & \text{if } n = k \\ 0 & \text{if } n < k \end{cases} \quad (5)$$

S4 is a deep SSM which is build with four ideal components for time series analysis, specifically, long sequences. First of all, it contains the continuous representation of SSMs previously revised in Eq. (4), for which with the help of HiPPO matrices [18], it provides an importance score for each past time step thought an online compression of signals and a novel and robust updating system (HiPPO-LegS) that scale for long sequences. In a nutshell, HiPPO aims to overcome the issue of time series of different length and the vanishing gradient problem. HiPPO is referenced in Eq. (5), which compress the scaled Legendre measure (LegS) operator for an uniformly system update on the SMM vector A .

$$\begin{aligned} \bar{A} &= (I - \Delta/2 \cdot A)^{-1} (I + \Delta/2 \cdot A) \\ \bar{B} &= (I - \Delta/2 \cdot A)^{-1} \Delta B \\ \bar{C} &= C \end{aligned} \quad (6)$$

Additionally, HiPPO architecture provides the advantage of being able to handle irregularly sampled data with the help of a recurrent discretization procedure by a step size Δ using the bilinear method. The Eq. (6) discretization procedure creates a sequence-to-sequence mapping that yields a recurrent state space; here, the SSMs can be computed like an RNN. Concretely, it can be viewed as a hidden state with a transition matrix \bar{A} .

$$\begin{aligned} y_k &= \bar{C} \bar{A}^k u_0 + \bar{C} \bar{A}^{k-1} u_1 + \dots \\ &\quad + \bar{C} \bar{A} \bar{B} u_{k-1} + \bar{C} \bar{B} u_k \\ &= \bar{C} \bar{K} * u \end{aligned} \quad (7)$$

$$\begin{aligned} \bar{k} \in \mathbb{R}^L &:= K_L(\bar{A}, \bar{B}, \bar{C}) := (\bar{C} \bar{A}^i)_{i \in [L]} \\ &= (\bar{C} \bar{B}, \bar{C} \bar{A} \bar{B}, \dots, \bar{C} \bar{A}^{L-1} \bar{B}) \end{aligned} \quad (8)$$

The RNN described previously can be transformed into a CNN by unrolling in the discrete convolution step, which is shown in Eq. (7), where a single convolution can be computed efficiently with fast Fourier transform given the SSM convolution kernel \bar{K} represented in Eq. (8), which can be computed in a way that is amenable to

an . We strongly encourage the reader to refer to [19] and [18] for further investigation towards S4 model and its components. From an external perspective, however, the S4 layer that is composed of multiple S4 blocks can be considered as a drop-in replacement for one-dimensional (potentially) dilated convolutional layer, RNNs or transformer layers, which is particularly adapted to the requirements of time series analysis.

2) Performance Metrics:

$$MAE = \frac{1}{n} \sum_{t=1}^n \sum_{k=1}^K |(y - \hat{y}) \odot m_{\text{eval}}|_{t,k} \quad (9)$$

$$MSE = \frac{1}{n} \sum_{t=1}^n \sum_{k=1}^K ((y - \hat{y}) \odot m_{\text{eval}})_{t,k}^2 \quad (10)$$

$$RMSE = \sqrt{\frac{1}{n} \sum_{t=1}^n \sum_{k=1}^K ((y - \hat{y}) \odot m_{\text{eval}})_{t,k}^2} \quad (11)$$

$$MRE = \frac{1}{n} \sum_{t=1}^n \sum_{k=1}^K m_{\text{eval}}|_{t,k} \frac{|(y - \hat{y})|_{t,k}}{|y_{t,k}|} \quad (12)$$

$$CRPS = \frac{\sum_{t=1}^n \sum_{k=1}^K m_{\text{eval}}|_{t,k} \frac{2}{|A|} \sum_{\alpha \in A} \Lambda_{\alpha}(F^{-1}(a)_{t,k}, y_{t,k})}{\sum_{t=1}^n \sum_{k=1}^K m_{\text{eval}}|_{t,k} |y_{t,k}|} \quad (13)$$

This section describes the performance metrics used throughout this work. We use a wide range of performance metrics for the computation of errors between targets and imputed values ($e_t = y - \hat{y}$), where for y and \hat{y} we apply the respective conditional masking for metrics computation ($m_{\text{eval}} = m_{\text{mvi}} \odot (1 - m_{\text{imp}})$).

Firstly, from a deterministic perspective, specifically for the computation of absolute errors we implemented mean absolute error (MAE) (9) which is determined by dividing the total absolute errors by the total sample size of observations n . For the account of larger error sensitivity we implemented mean squared error (MSE) (10) which is the sum $\sum_{t=1}^n$ of squared errors e_t^2 divided by the total sample size of observations n , similarly, we implemented root mean squared error (RMSE) (11) to account for larger errors while preserving the error ranges in proportion to the observed mean, and to measure the precision of our imputations mean relative error (MRE) which as a percentage representation computes the mean of differences between the absolute errors $|y - \hat{y}|$ divided by their target values y .

Finally, due to the stochasticity of our proposed methods, we are also interested on probabilistic metrics, such as the Continuous Ranked Probability Score (CRPS) (13), which assesses the compatibility of a probability distribution F with an observation y . CRPS is then defined as the integral of the quantile loss $\Lambda_{\alpha}(q, y) := (\alpha - \mathbb{1}_{y < q})(y - q)$ over all thresholds $\alpha \in [0, 1]$, i.e.

$$CRPS(F^{-1}(\alpha), x) = \int_0^1 2\Lambda_{\alpha}(F^{-1}(\alpha), x) d\alpha. \quad (14)$$

In practice, we approximate the distribution F through a finite number of imputation samples and approximate the integral through a finite sum over 19 quantile values $\alpha \in A := \{0.05, 0.10, \dots, 0.95\}$. Finally, the metric we refer to as CRPS, as defined in (13), refers to the normalized average of the CRPS (across time steps and features) with appropriate masking.

Table XVIII
RESULTS FOR THE ABLATION STUDY.

20% BM on PTB-XL			
Setting	MAE	RMSE	CRPS
A	0.0435 \pm 3e-3	0.1167 \pm 1e-2	0.3181 \pm 1e-2
B	0.0367 \pm 2e-3	0.0929 \pm 2e-2	0.2817 \pm 2e-2
C	0.0324\pm3e-3	0.0832\pm8e-3	0.2689\pm3e-3

D. Additional results

1) *Ablation study*: Table XVIII contains the results obtained for an ablation study done aiming to find the best configuration for an S4 layer in our proposed model. We present three different variants with capital letter notations. (A) represents a DiffWave imputer with dilated convolutional layers. (B) represents a diffwave imputer with a S4 layer in replacement of the dilated convolutional layer. (C) represents setting B and an extra S4 layer after the conditional data addition (SSSD^{S4}). The experiment was carried out in a BM scenario at 20% of missing values on the PTB-XL data set. Metrics were obtained at the 150,000 training iterations. We report an averaged MAE, RMSE and CRPS over three trials for 10 samples generated for each sample of the test set. The results observed in table XVIII shows the metrics obtained for three different variants in our ablation study.

From the above results, we observe improvements over deterministic and probabilistic metrics that are leads by a replacement of dilated convolutional layers with state space models specifically the S4 models within a DiffWave imputer architecture, while the main improvement is over the use of a single S4 model overcome the use dilated convolutional layers, the use of a second state space model after the addition of conditional information also achieves better results, thus, letting us to propose (C) variant as the SSSD^{S4} model for time series imputation and forecasting.

2) *Full imputation and forecasting results*: In Table XIX to Table XXIII, we compile the full imputation and forecasting results including all available baseline results and missingness scenarios that were only presented in an excerpted fashion in the main text. In addition, Table XXIV and Table XXV describe the number of training iterations used while training on each of the data sets.

Table XIX
IMPUTATIONS FOR RM, MNR, AND BM SCENARIOS ON THE PTB-XL DATA SET.

Model	MAE	RMSE	CRPS
20% RM on PTB-XL			
Median	0.1040	0.2071	0.9607
LAMC	0.0678	0.1309	0.6828
DiffWave D_0	0.0047 \pm 2e-5	0.0175 \pm 3e-4	0.0317 \pm 1e-4
DiffWave D_1	0.0043 \pm 4e-4	0.0177 \pm 4e-4	0.0305 \pm 1e-3
CSDI	0.0038 \pm 2e-6	0.0189 \pm 5e-5	0.0265 \pm 6e-6
CSDI ^{S4}	0.0031\pm1e-7	0.0171 \pm 6e-4	0.0202\pm1e-5
SSSD ^{SA} D_0	0.0052 \pm 3e-5	0.0229 \pm 4e-6	0.0338 \pm 1e-4
SSSD ^{SA} D_1	0.0045 \pm 3e-7	0.0181 \pm 4e-6	0.0314 \pm 7e-5
SSSD ^{S4} D_0	0.0044 \pm 2e-5	0.0137 \pm 1e-4	0.0284 \pm 2e-3
SSSD ^{S4} D_1	0.0034 \pm 4e-6	0.0119\pm1e-4	0.0282 \pm 1e-3
20% MNR on PTB-XL			
Median	0.1074	0.2157	0.9652
LAMC	0.0759	0.1498	0.8345
DiffWave D_0	0.0482 \pm 1e-3	0.1209 \pm 8e-3	0.3411 \pm 1e-2
DiffWave D_1	0.0250 \pm 1e-3	0.0808 \pm 5e-3	0.1610 \pm 1e-2
CSDI	0.0186 \pm 1e-5	0.0435 \pm 2e-4	0.1306 \pm 5e-5
CSDI ^{S4}	0.0222 \pm 2e-5	0.0573 \pm 1e-3	0.1392 \pm 4e-2
SSSD ^{SA} D_0	0.0202 \pm 1e-3	0.0612 \pm 1e-2	0.1029 \pm 7e-3
SSSD ^{SA} D_1	0.0170 \pm 1e-4	0.0492 \pm 1e-2	0.1152 \pm 1e-5
SSSD ^{S4} D_0	0.0116 \pm 2e-4	0.0251 \pm 7e-4	0.0792 \pm 4e-4
SSSD ^{S4} D_1	0.0103\pm3e-3	0.0226\pm9e-4	0.0787\pm3e-3
20% BM on PTB-XL			
Median	0.1252	0.2347	0.9819
LAMC	0.0840	0.1171	0.9999
DiffWave D_0	0.0492 \pm 1e-3	0.1405 \pm 8e-3	0.2975 \pm 4e-3
DiffWave D_1	0.0451 \pm 7e-4	0.1378 \pm 5e-3	0.3520 \pm 1e-2
CSDI	0.1054 \pm 4e-5	0.2254 \pm 7e-5	0.7468 \pm 2e-4
CSDI ^{S4}	0.0792 \pm 2e-4	0.1879 \pm 1e-4	0.6222 \pm 6e-4
SSSD ^{SA} D_0	0.0493 \pm 1e-3	0.1192 \pm 7e-3	0.3251 \pm 6e-3
SSSD ^{SA} D_1	0.0435 \pm 3e-3	0.1167 \pm 1e-2	0.3181 \pm 1e-2
SSSD ^{S4} D_0	0.0415 \pm 1e-3	0.1073 \pm 5e-3	0.2715 \pm 7e-3
SSSD ^{S4} D_1	0.0324\pm3e-3	0.0832\pm8e-3	0.2689\pm3e-3

Table XX

RM IMPUTATION RESULTS FOR THE ELECTRICITY DATA SET. OVERALL, CSDI^{S4} OUTPERFORMED ALL THE RM SCENARIOS' BASELINES METRICS EVEN AT HIGH LEVELS OF MISSING DATA. ALL BASELINE RESULTS WERE COLLECTED FROM [12]

10% RM on Electricity			
Model	MAE	RMSE	MRE
Median	2.056	2.732	110%
M-RNN	1.244	1.867	66.6%
GP-VAE	1.094	1.565	58.6%
BRITS	0.847	1.322	45.3%
Transformer	0.823	1.301	44.0%
SAITS	0.735	1.162	39.4%
SSSD^{S4}	0.345±1e-4	0.554±5e-5	18.4%±5e-5
30% RM on Electricity			
Model	MAE	RMSE	MRE
Median	2.055	2.732	110%
M-RNN	1.258	1.876	67.3%
GP-VAE	1.057	1.571	56.6%
BRITS	0.943	1.435	50.4%
Transformer	0.846	1.321	45.3%
SAITS	0.790	1.223	42.3%
SSSD^{S4}	0.407±5e-4	0.625±1e-4	21.8%±0%
50% RM on Electricity			
Model	MAE	RMSE	MRE
Median	2.053	2.728	109%
M-RNN	1.283	1.902	68.7%
GP-VAE	1.097	1.572	58.8%
BRITS	1.037	1.538	55.5%
Transformer	0.895	1.410	47.9%
SAITS	0.876	1.377	46.9%
SSSD^{S4}	0.532±1e-4	0.821±1e-4	28.5%±1e-4

Table XXI
MAE, MSE, MRE FOR PEM-S-BAY AND METR-LA DATA SETS. ALL BASELINE RESULTS WERE COLLECTED FROM [9].

25% RM on PEMS-Bay			
Model	MAE	MSE	MRE%
Mean	5.42±0.00	86.59±0.00	8.67±0.00
KNN	4.30±0.00	49.80±0.00	6.88±0.00
MF	3.29±0.01	51.39±0.64	5.27±0.02
MICE	3.09±0.02	31.43±0.41	4.95±0.02
VAR	1.30±0.00	6.52±0.01	2.07±0.01
rGAIN	1.88±0.02	10.37±0.20	3.01±0.04
BRITS	1.47±0.00	7.94±0.03	2.36±0.00
MPGRU	1.11±0.00	7.59±0.02	1.77±0.00
GRIN	0.67±0.00	1.55±0.01	1.08±0.00%
SSSD^{S4}	0.97±0.01	2.98±0.03	1.42±0.01
25% RM on METR-LA			
Model	MAE	MSE	MRE%
Mean	7.56±0.00	142.22±0.00	13.10±0.00
KNN	7.88±0.00	129.29±0.00	13.65±0.00
MF	5.56±0.03	113.46±1.08	9.62±0.05
MICE	4.42±0.07	55.07±1.46	7.65±0.12
VAR	2.69±0.00	21.10±0.02	4.66±0.00
rGAIN	2.83±0.01	20.03±0.09	4.91±0.01
BRITS	2.34±0.00	16.46±0.05	4.05±0.00
MPGRU	2.44±0.00	22.17±0.03	4.22±0.00
GRIN	1.91±0.00	10.41±0.03	3.30±0.00
SSSD^{S4}	2.83±0.02	21.95±0.14	5.59±0.08

Table XXII
FORECASTING RESULTS FOR THE PTB-XL DATA SET.

TF on PTB-XL			
Model	MAE	RMSE	CRPS
Median	0.134	0.273	0.953
CSDI	0.165±0.0009	0.302±0.0004	1.064±0.002
CSDI ^{S4}	0.120±0.0002	0.246±0.0001	0.826±0.0002
SSSD ^{SA}	0.087±0.008	0.220±0.012	0.557±0.051
SSSD ^{S4}	0.090±0.003	0.219±0.006	0.633±0.010

Table XXIII
TIME SERIES FORECASTING MAE AND MSE ON THE ETTM1 DATA SET.

Model	24	48
LSTNet	1.170 1.968	1.215 1.999
LSTMa	0.629 0.621	0.939 1.392
Reformer	0.607 0.724	0.777 1.098
LogTrans	0.412 0.419	0.583 0.507
Informer†	0.371 0.306	0.470 0.465
Informer	0.369 0.323	0.503 0.494
SSSD^{S4}	0.361(6) 0.351(9)	0.479(8) 0.612(2)
Model	96	288
LSTNet	1.542 2.762	2.076 1.257
LSTMa	0.913 1.339	1.124 1.740
Reformer	0.945 1.433	1.094 1.820
LogTrans	0.792 0.768	1.320 1.462
Informer†	0.612 0.681	0.879 1.162
Informer	0.614 0.678	0.786 1.056
SSSD^{S4}	0.547(12) 0.538(13)	0.648(10) 0.797(5)
Model	672	
LSTNet	2.941 1.917	
LSTMa	1.555 2.736	
Reformer	1.232 2.187	
LogTrans	1.461 1.669	
Informer†	1.103 1.231	
Informer	0.926 1.192	
SSSD^{S4}	0.783(66) 0.804(45)	

Table XXIV
TRAINING ON THE PROPOSED PTB-XL DATA SETS. TRAINING EPOCHS (E) AND ITERATIONS (I) ON THE PROPOSED PTB-XL DATA SET

Model	PTB 248	PTB 1000
CSDI	200 (e)	200 (e)
CSDI ^{S4}	200 (e)	200 (e)
DiffWave	150,000 (i)	150,000 (i)
SSSD ^{SA}	150,000 (i)	150,000 (i)
SSSD ^{S4}	150,000 (i)	150,000 (i)

Table XXV

$SSSD^{S4}$ TRAINING ON BENCHMARKING DATA SETS. CONTAINS THE $SSSD^{S4}$ TRAINING ITERATIONS (i) ON THE BENCHMARKING DATA SETS ACROSS DIVERSE BASELINES.

data set	Setting	Iterations
Electricity	Imputation 10%	150,000 (i)
Electricity	Imputation 30%	150,000 (i)
Electricity	Imputation 50%	150,000 (i)
PEMS-BAY	Imputation 25%	350,000 (i)
METR-LA	Imputation 25%	250,000 (i)
MuJoCo	Imputation 70%	232,000 (i)
MuJoCo	Imputation 80%	160,000 (i)
MuJoCo	Imputation 90%	150,000 (i)
Solar	Forecast 24	100,000 (i)
ETTm1	Forecast 24	212,000 (i)
ETTm1	Forecast 48	150,000 (i)
ETTm1	Forecast 96	250,000 (i)
ETTm1	Forecast 288	250,000 (i)
ETTm1	Forecast 672	250,000 (i)

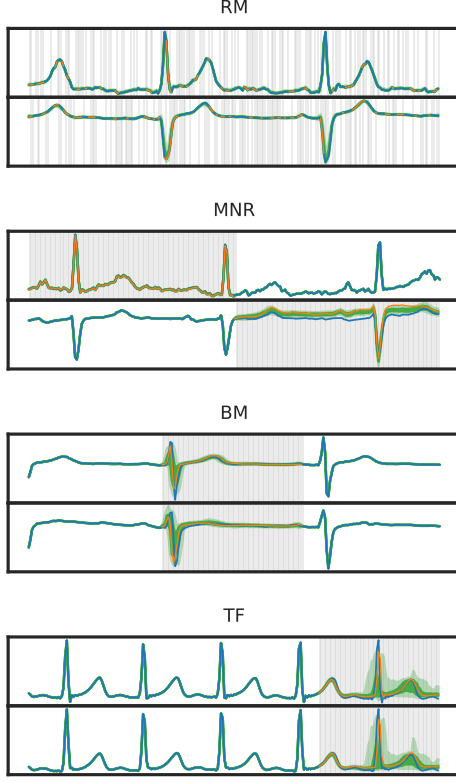


Figure 4. Color scheme introduction. The proposed model $SSSD^{S4}$ provides imputations for different missingness scenarios that are not only quantitatively but even qualitatively superior, see below, on different data sets for different missingness scenarios (RM: random missing, MNR: missing not at random, BM: blackout missing TF: time series forecasting). Similarly, The signal is in blue, where the white background represents the conditioned ground truth, whereas the gray background represents the target signal. Prediction bands derived from 100 imputations represent quantiles from 0.05 to 0.95 as lighter shaded green and from 0.25 to 0.75 as darker shaded green. As these bands do not allow visually assessing the quality of individual imputations, we always additionally show a randomly selected single sample in orange.

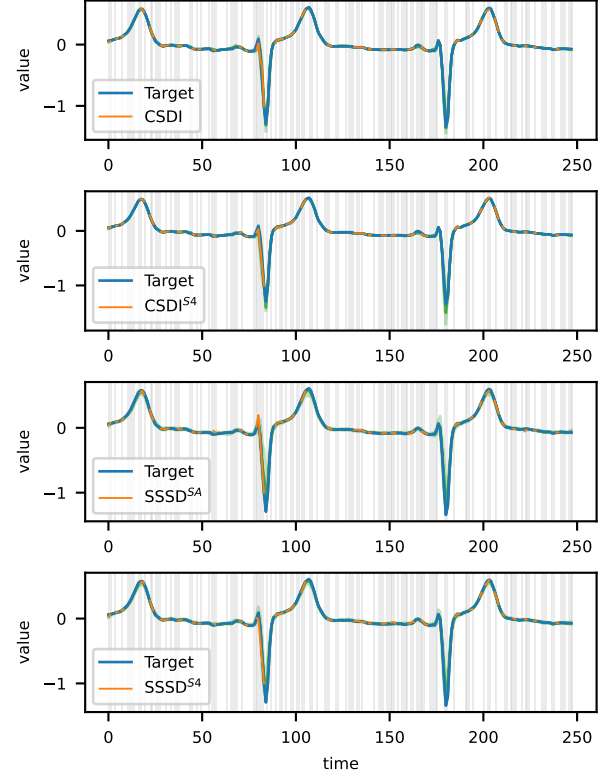


Figure 5. PTB-XL RM imputations of a V3 lead for an ECG from a patient with a anterior myocardial infarction (AMI). The figure demonstrate 100 RM imputations on a single sample tested at 50% for four imputers on the PTB-XL data set. As clearly seen from the the plots above, all the diffusion models are highly capable of reconstructing time series, even when there is a high ratio of missing values in a RM scenario. Quantitatively, as seen in the main paper, we observed that $CSDI^{S4}$ outperforms the rest of the models on this data set. The differences in terms of imputation quality can hardly be observed visually as the rest of the models present slight green shaded areas surrounding the orange imputed areas which represent the imputations quantiles.

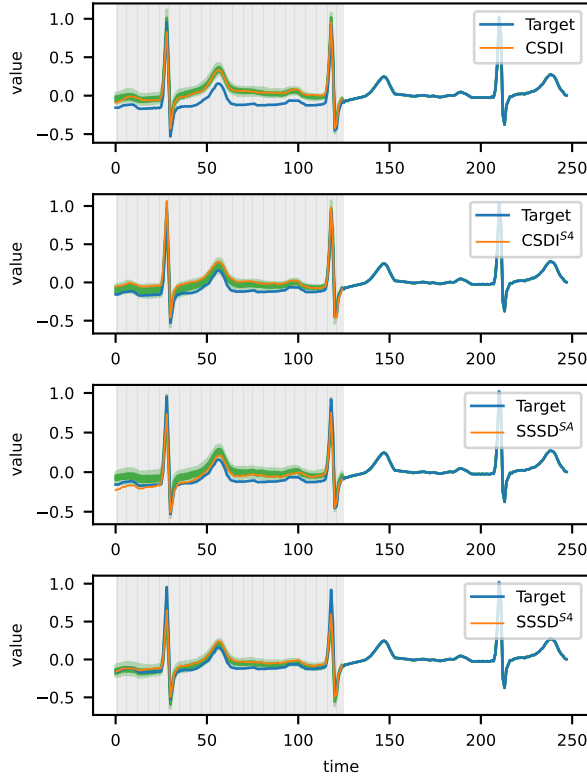


Figure 6. PTB-XL MNR imputations of a V4 lead for an ECG from a patient an AV block (AVB). The figure demonstrate 100 MNR imputations on a single sample tested at 50% for four imputers on the PTB-XL data set. As previously discussed, MNR assumes that the missing blocks are located at different time steps on each feature. Technically, on this setting, the diffusion models are capable of deriving the missing segments in a given channel from neighboring channels at the same time steps, which empirically seems to be a factor that enables an overall very good reconstruction across all models.

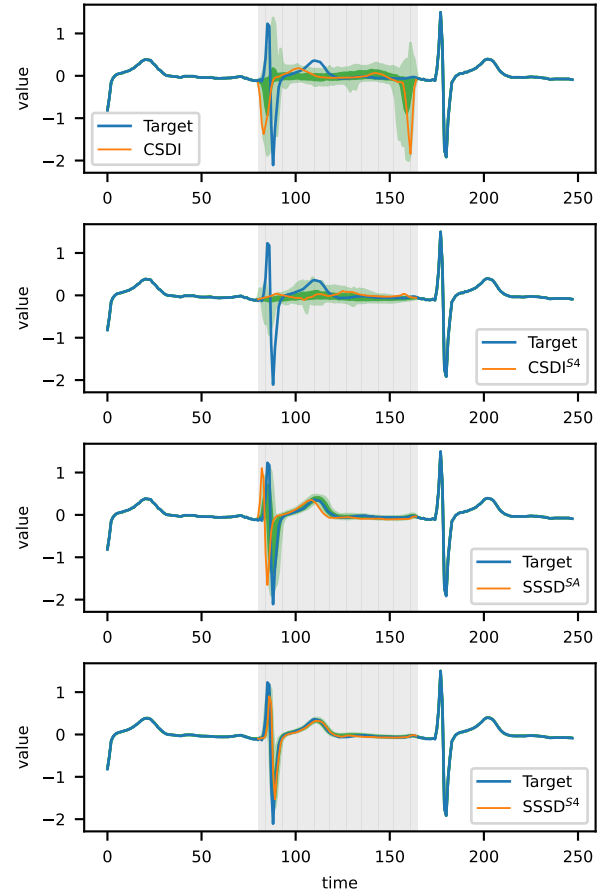


Figure 7. PTB-XL BM imputations for lead V2 for an ECG collected from a healthy patient. The figure demonstrate four BM imputations tested at 30% on the PTB-XL data set reiterating the qualitative differences in imputation quality already demonstrated in the main text.

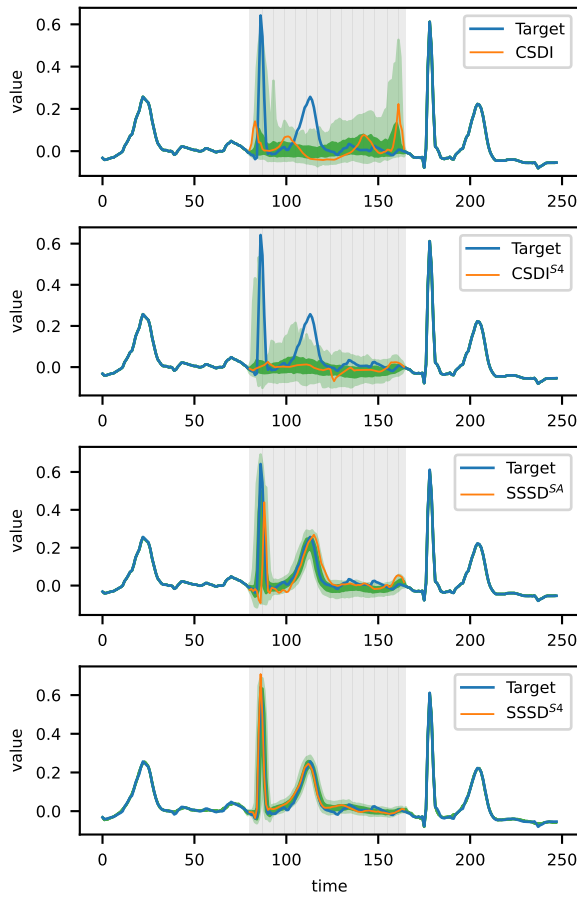


Figure 8. PTB-XL BM imputations for lead V6 for a normal heart condition. The figure demonstrate four BM imputations tested at 30% on the PTB-XL data set.

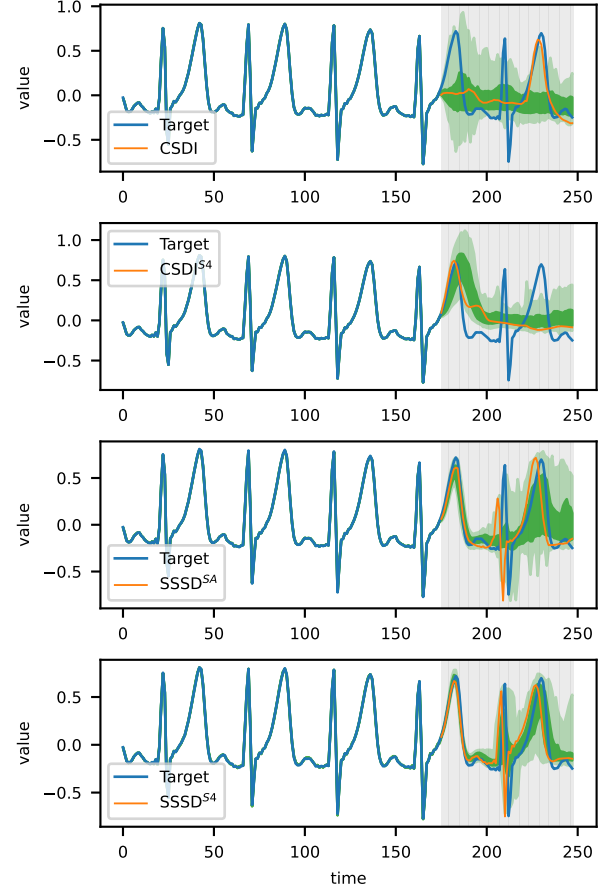


Figure 9. PTB-XL TF for lead V3 for a patient with left ventricular hypertrophy. The figure demonstrate 100 BM imputations on a single sample tested at 50% for four imputers on the PTB-XL data set. CSDI model is overall learning the trend that the series have, with a few correct feature generations as seen in the plot, nevertheless, we observe that the imputation falls outside the 0.05 and 0.95 quantile range, which is basically an outlier. CSDI^{S4} improves the quality of the generations, as its quantiles are less diverse and start to follow the signals patterns, however, it seems that after certain number of steps, the learning decrease dramatically. On the other side SSSD^{SA} and SSSD^{S4} correctly capture characteristics of the signal. In particular, SSSD^{S4} maintains a tight interquartile range even at longer forecasting horizons.

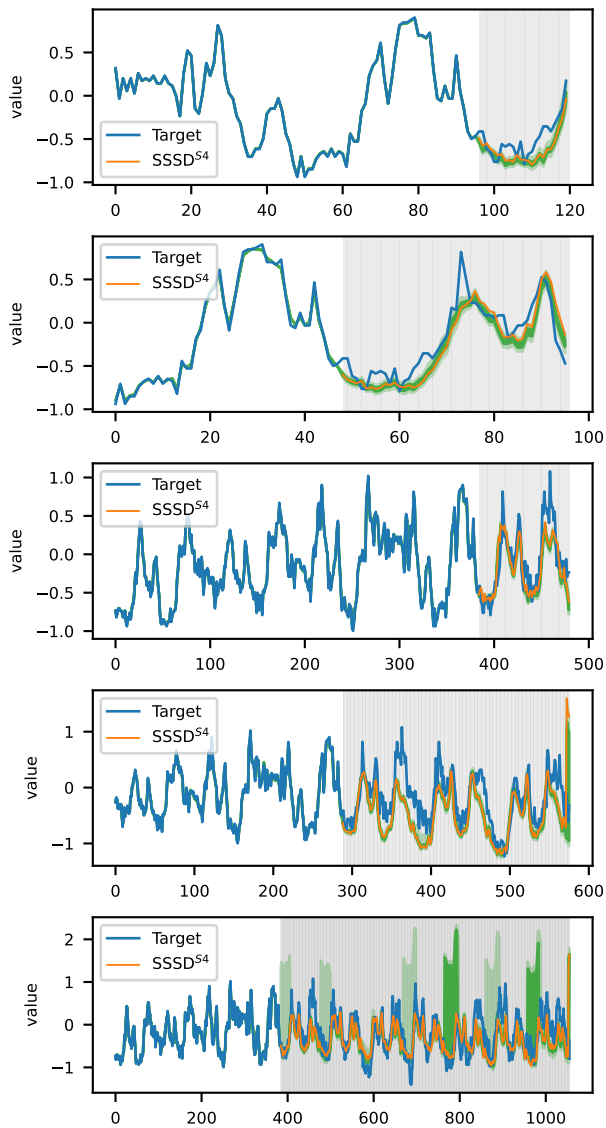


Figure 10. ETTm1 TF for the five different forecasting settings. From top to bottom 24, 48, 96, 288, 384 forecasting horizon targets. These plots display the complete sample including the conditional part, see figure for a more detailed plots of only the imputed area.

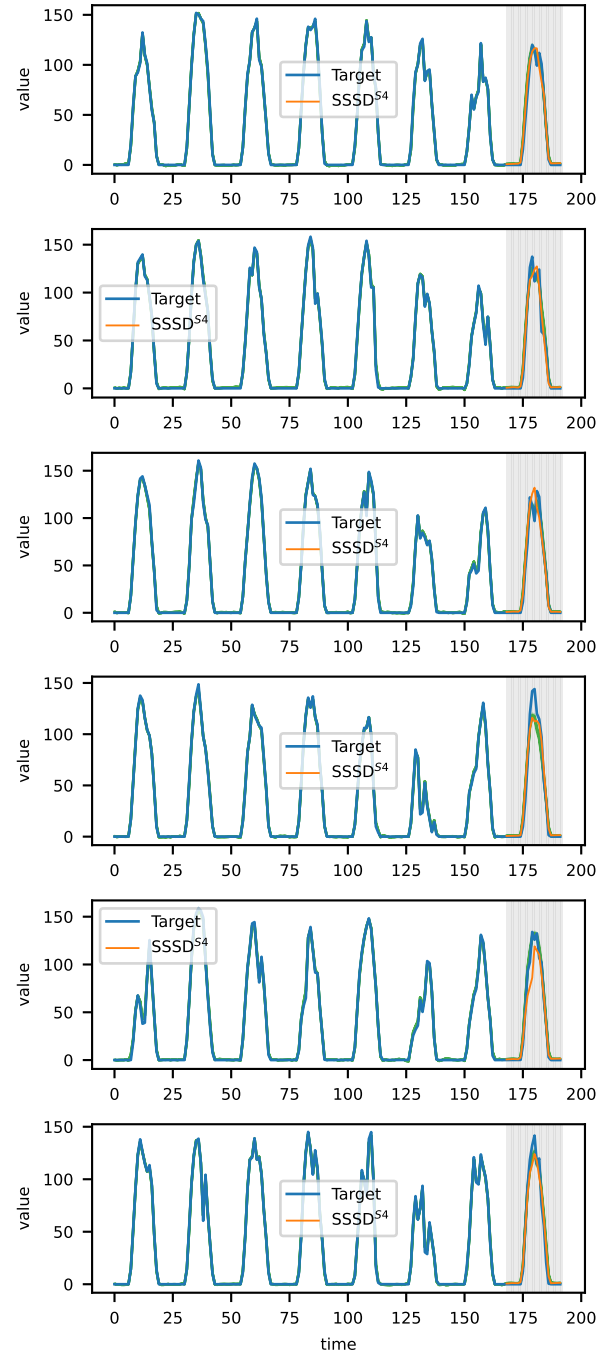


Figure 11. TF for six different channels of the Solar data set. These plots display the complete sample including the conditional part, see figure 12 for a more detailed plots of only the imputed area.

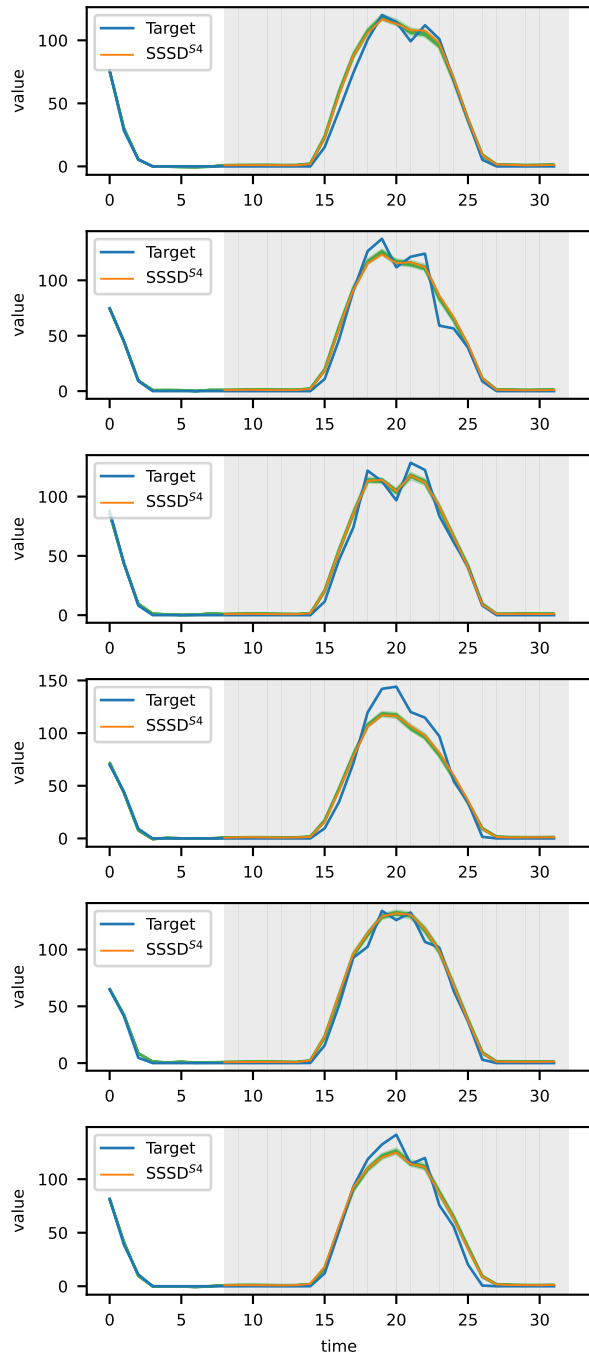


Figure 12. TF for six different channels of the Solar data set. These plots display only the target generated area.